Journal of Solid State Chemistry 183 (2010) 356–360

Contents lists available at ScienceDirect

Journal of Solid State Chemistry

journal homepage: www.elsevier.com/locate/jssc

Solvothermal indium fluoride chemistry: Syntheses and crystal structures of $K_5In_3F_{14}$, β-$(NH_4)_3InF_6$ and $[NH_4]_3[C_6H_{21}N_4]_2[In_4F_{21}]$

Anil C.A. Jayasundera [a], Richard J. Goff [a], Yang Li [a], Adrian A. Finch [b], Philip Lightfoot [a,*]

[a] EaStChem, School of Chemistry, University of St Andrews, St Andrews, Fife KY16 9ST, UK
[b] School of Geography and Geosciences, University of St Andrews, St Andrews, Fife KY16 9AL, UK

ARTICLE INFO

Article history:
Received 12 August 2009
Received in revised form
10 November 2009
Accepted 23 November 2009
Available online 2 December 2009

Keywords:
Solvothermal synthesis
Indium fluoride
Chiolite
Cryolite
Hybrid material

ABSTRACT

The solvothermal syntheses and crystal structures of three indium fluorides are presented. $K_5In_3F_{14}$ (**1**) and β-$(NH_4)_3InF_6$ (**2**) are variants on known inorganic structure types chiolite and cryolite, respectively, with the latter exhibiting a complex and apparently novel structural distortion. $[NH_4]_3[C_6H_{21}N_4]_2[In_4F_{21}]$ (**3**) represents a new hybrid composition displaying a unique trimeric metal fluoride building unit.

1. Introduction

Solvothermal chemistry is a well-established route to interesting new compositions and crystal structure types, including those which are not amenable by solid state syntheses. Nevertheless, there are vast regions of composition space which have not yet been explored, either hydrothermally or, more generally, solvothermally. Amongst the trivalent metal fluorides, for example, there is a reasonably extensive literature on aluminium fluorides, which generally employ organic 'structure-directing' agents [1–3]. For the remaining Groups 13 and 3 metals, these systems are much less well-explored. The current Cambridge Database [4], lists around 12 discrete compounds having a metal, *M*, bonded only to fluoride (where *M*=Ga, In, Sc or Y). We have recently been exploring some of these systems in order to identify novel fluoride-based materials as potential hosts for luminescent lanthanide ions. This has led to the characterisation of the first organically templated yttrium fluorides [5,6] scandium fluorides [7,8] and the first example of an indium fluoride with the capacity to host active luminescent lanthanides [9]. The indium fluoride in the latter example, $[C_4H_{14}N_2][InF_5]$, was the first case of an infinitely connected indium fluoride unit in hybrid systems, the previous examples all exhibiting only isolated $[InF_6]^{3-}$ octahedral units [10,11]. In^{3+} is an interesting entity structurally, as it has an ionic radius (in 6-coordination) of 0.80 Å, intermediate between that of Sc^{3+} (0.745 Å) and the smallest of the lanthanides, Lu^{3+} (0.86 Å). In order to further expand on the structural architectures known in solvothermal indium fluoride chemistry we now present three further examples of our exploratory searches in this field. The first two compounds, $K_5In_3F_{14}$ (**1**) and β-$(NH_4)_3InF_6$ (**2**), are variants on known inorganic structure types chiolite and cryolite, whereas the third, $[NH_4]_3[C_6H_{21}N_4]_2[In_4F_{21}]$ (**3**), represents a novel hybrid composition displaying a unique trimeric metal fluoride building unit.

2. Experimental

2.1. Synthesis

All three of the title compounds were synthesised by solvothermal reaction. The starting materials were InF_3 (99.99%, Acros Organic), $In(NO_3)_3 \cdot 5H_2O$ (99.999%, Aldrich), hydrofluoric acid, (HF(aq), 48% wt, Aldrich), tris(2-aminoethyl)amine (*tren*) $[(NH_2CH_2CH_2)_3N$, 99.99%, Aldrich], $NaNO_3$ (99%, Aldrich), K_2CO_3 (99%, Aldrich), ethylene glycol (99.5%, Aldrich) and ethanol (99%, Alfa-Aesar). For **1**, K_2CO_3 (0.318 g, 1 mmol) and $In(NO_3)_3 \cdot 5H_2O$ (0.391 g, 1 mmol) were placed in a 40 ml Teflon-lined stainless steel autoclave with 0.2 ml (10 mmol) HF, 3.0 ml (50 mmol) ethanol and 3.0 ml (55 mmol) ethylene glycol. The autoclave was heated at 190 °C for one day. This reaction produced a pure

* Corresponding author.
E-mail addresses: pl@st-andrews.ac.uk, pl@st-and.ac.uk (P. Lightfoot).

0022-4596/$ - see front matter © 2009 Elsevier Inc. All rights reserved.
doi:10.1016/j.jssc.2009.11.022

Table 1
Crystallographic data for $K_5In_3F_{14}$ **1**, β-$(NH_4)_3InF_6$ **2** and $[NH_4]_3[C_6H_{21}N_4]_2[In_4F_{21}]$ **3**.

	1	2	3
Formula	$K_5In_3F_{14}$	$(NH_4)_3InF_6$	$[NH_4]_3[C_6H_{21}N_4]_2[In_4F_{21}]$
F_w	805.96	282.93	1210.94
Space group	$P4/nmc$	$P2_1/c$	$P6_3/m$
a (Å)	7.910(2)	11.5164(7)	11.7670(9)
b (Å)	$=a$	6.4926(4)	$=a$
c (Å)	11.883(3)	11.5438(6)	14.7670(12)
β (deg)		111.38(11)	
V (Å^3)	743.6(4)	803.77(7)	1770.7(2)
T (K)	113	113	113
Z	2	4	2
Total/unique reflns	4436/424	7920/1837	12032/1386
Obsd data [$I > 2\sigma(I)$]	369	1502	1204
Restraints/parameters	0/32	0/130	10/92
$R1$, w$R2$ ($I > 2\sigma(I)$)	0.027/0.113	0.029/0.081	0.065/0.180
$R1$, w$R2$ (all data)	0.031/0.120	0.036/0.085	0.082/0.217

Table 2
Selected bond lengths (Å).

1	2	3
In(1)–F(1) × 2 2.105(4)	In(1)–F(1) × 2 2.065(3)	In(1)–F(1) × 2 2.074(5)
In(2)–F(2) × 4 2.034(3)	In(1)–F(2) × 2 2.086(2)	In(1)–F(2) 2.034(5)
	In(1)–F(3) × 2 2.078(2)	In(1)–F(3) 2.104(5)
In(2)–F(1) × 4 2.081(4)		In(1)–F(3) 2.122(4)
In(2)–F(3) × 2 2.055(8)	In(2)–F(4) × 2 2.095(2)	In(1)–F(4) 2.030(5)
	In(2)–F(5) × 2 2.046(3)	
K(1)–F(1) × 2 3.147(2)	In(2)–F(6) × 2 2.084(2)	In(2)–F(5) × 6 2.074(4)
K(1)–F(2) × 2 2.595(4)		
K(1)–F(2) × 2 2.599(4)		
K(1)–F(3) × 2 2.973(2)		
K(2)–F(2) × 8 2.939(5)		

polycrystalline sample; single crystals were prepared via a minor modification of the above, using a mixed ethylene glycol/water co-solvent (8 ml) heated at 220 °C for three days (the sample in this case was not phase pure). For **2**, InF_3 (0.1718 g, 1.0 mmol) was placed in a polypropylene bottle with 2.0 ml (100 mmol) HF and 5.0 ml H_2O. This was heated at 100 °C for an hour, and then the contents were transferred into a Teflon-lined stainless steel autoclave, with the addition of 0.5 ml (3.5 mmol) of *tren* and 5 ml (100 mmol) ethylene glycol. The autoclave was heated at 190 °C for five days. For **3**, InF_3 (0.1718 g, 1 mmol), $NaNO_3$ (0.1669 g, 2.0 mmol) and *tren* (0.8 ml, 5.5 mmol) were placed in a Teflon-lined stainless steel autoclave with 0.2 ml (10 mmol) HF and 2.5 ml (45 mmol) ethanol. The autoclave was heated at 190 °C for four days. All products were filtered, washed with distilled water and dried at room temperature to give colourless crystals. Phase purity was studies using standard elemental analysis, energy-dispersive X-ray analysis (EDX) and powder X-ray diffraction (PXRD). Elemental analysis for **3**, $[NH_4]_3[C_6H_{21}N_4]_2[In_4F_{21}]$, obs. (calc.): C: 11.42% (11.90%), H: 3.79% (4.50%), N: 10.85% (12.72%). EDX confirmed the absence of Na and O. PXRD (supplementary material) showed a good match between the bulk product and the observed crystal structure in each case, though in **2** it is apparent that the room-temperature structure may exhibit higher symmetry than the phase determined by the present single crystal experiment.

2.2. Characterisation

PXRD was carried out on a Stoe STADI/P transmission diffractometer using Cu$K\alpha$1 radiation, with a 2θ range of 5–100° and a data collection time of 15 h. SEM/EDX studies (for qualitative analyses) were carried out on a Jeol JSM 5600. Single-crystal X-ray diffraction data were collected using a Rigaku Mercury CCD equipped with graphite monochromated Mo$K\alpha$ radiation at 113 K. The structures were solved by direct methods and refined by standard techniques, using the SHELX-97 [12] and WinGX [13] packages. All non-hydrogen atoms were refined with anisotropic thermal parameters. Hydrogen atoms attached to organic moieties were located at geometrically calculated positions and refined with isotropic thermal parameters; those forming NH_4^+ groups were located and refined with fixed isotropic thermal parameters. Other crystal data and experimental parameters are summarised in Table 1.

3. Results and discussion

For each structure, the crystallographic details are given in Table 1 and selected bond lengths in Table 2.

3.1. $K_5In_3F_{14}$ (**1**)

The crystal structure of **1** is a variant of the chiolite structure (archetype $Na_5Al_3F_{14}$ [14]). The structure consists of layers of corner-linked InF_6 octahedra with one in every four octahedra 'missing' relative to a perovskite-like sheet; this missing octahedron is replaced by a larger K^+ ion in eight-fold coordination, K(2), such that a co-operative rotation of the In(1)F_6 octahedra around the a and b axes occurs to accommodate this (Fig. 1(a)). Further symmetry lowering from the maximum ideal symmetry ($I4/mmm$) occurs due to additional octahedral rotations around the c-axis. The $[KIn_3F_{14}]$ layers are separated by a further potassium site, K(1), also in eight-fold coordination (Fig. 1(b)).

$K_5In_3F_{14}$ has been prepared previously via a high-temperature solid state reaction [15]. The unit cell and space group was suggested based on PXRD, and is the same as reported here; atomic coordinates were not previously reported. The chiolite family includes oxides (eg. $Ca_5Te_3O_{14}$ [16], and oxyfluorides (eg. $Na_5W_3O_9F_5$ [17]) but is most prevalent amongst pure fluorides. ICSD contains five different compositions of the form $Na_5M_3^{3+}F_{14}$ (M^{3+}=Al, Ga, Cr, Mn and Fe) and one of composition $K_5M_3^{3+}F_{14}$ (M^{3+}=Ti). The recent single crystal study of $K_5V_3F_{14}$ [18] and the earlier reports of $K_5In_3F_{14}$ and $K_5Tl_3F_{14}$ [15] provide further data for comparison. Each of the four K-containing phases adopts the same variant of the structure-type, *viz.* space group $P4/mnc$, whereas amongst the Na-containing phases, only chiolite itself ($Na_5Al_3F_{14}$) adopts that symmetry. In the others the symmetry is lowered to orthorhombic ($Na_5Mn_3F_{14}$) or monoclinic. The reasons for these symmetry differences are not obvious, although presumably in $Na_5Mn_3F_{14}$ the Jahn-Teller preferences of Mn^{3+} may play a part. In the other cases, cation size effects will play some role, as is well known in perovskite chemistry. Considering the full series of ideal composition $A_5B_3F_{14}$, and using Shannon's [19] six-coordinate radii for B^{3+} and eight-coordinate radii for A^+, it can be seen that the tolerance of the K-containing series towards A/B size mismatch is much larger than that of the Na-containing series. The A/B ration varies from 2.19 (B=Al) down to 1.82 (B=Fe or Mn) for the Na-series and from 2.36 (B=V) down to 1.70 (B=Tl) for the K-series. In comparison with the Na-series, it might therefore be expected, based on this simplistic model, that $K_5In_3F_{14}$ (A/B=1.89) would be on the verge of a symmetry-lowering distortion, and $K_5Tl_3F_{14}$ should be within the lower-symmetry regime: a full structure analysis of the latter phase would be of interest. This structure determination of $K_5In_3F_{14}$ was

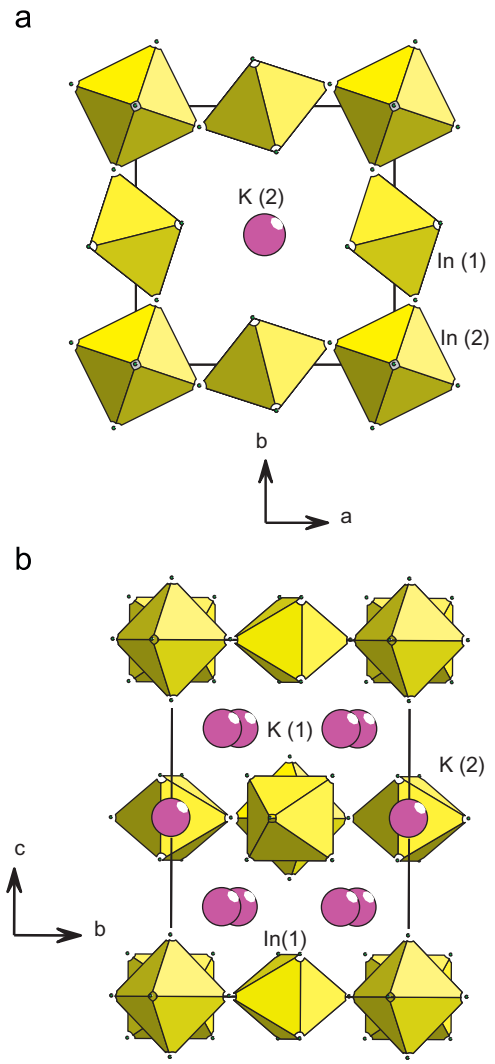

Fig. 1. (a) View of the chiolite structure of $K_5In_3F_{14}$ (**1**) down the *c*-axis, showing a single $[KIn_3F_{14}]$ layer. (b) Layer structure of 1 viewed along *a*.

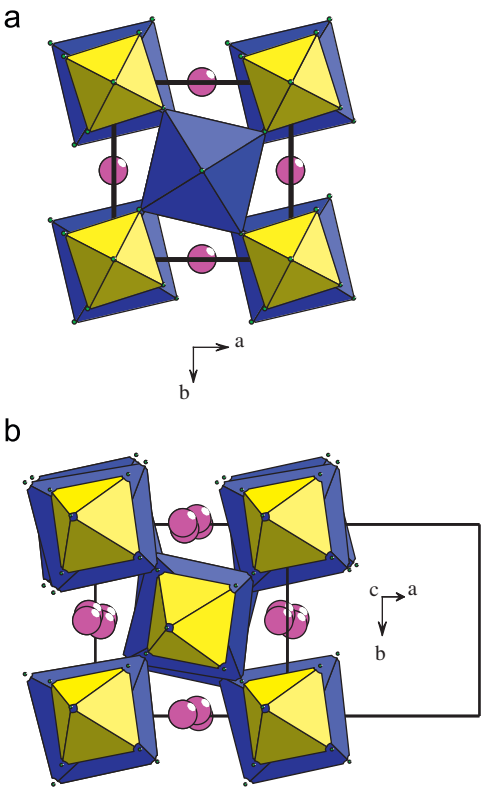

Fig. 2. (a) Tilt system in α-$(NH_4)_3InF_6$ [24]: octahedral tilts occur around the *c*-axis only. $(NH_4)^+$ cations on the *B*-sites shown in polyhedral format (larger polyhedra $(NH_4)F_6$, smaller polyhedra InF_6), those on the *A*-sites shown as spheres. (b) Tilt system in β-$(NH_4)_3InF_6$ (**2**): format as for Fig. 2(a). For comparison the cell is viewed along [10−1]. The additional tilts around the pseudo-cubic *a* and *b* axes and the displacements of the *A*-site cations can be seen.

carried out at 113 K. However, a second dataset, collected at 295 K, revealed no change in space group symmetry, and the overall structure is essentially unchanged in this temperature regime, with no increase of symmetry to the archetypal *I*4/*mmm*. So far, the only known example of this higher symmetry structure type is the high temperature paraelectric phase of the oxyfluoride $Na_5W_3O_9F_5$ [20].

3.2. *β-$(NH_4)_3InF_6$ (**2**)*

This phase is a novel variant of the cryolite structure type (archetype Na_3AlF_6 [21]); ie. a *B*-site ordered perovskite of the form $A_2(AB)X_6$. The compound arises due to the *in situ* breakdown of *tren* used in the reaction. Similar template decomposition has been observed in other *tren*/HF-containing reaction media [8]. The structural and phase transition behaviour observed in the cryolite family have been well discussed (see eg. Flerov et al. [22]). These compounds also form part of a much wider family of *B*-site ordered perovskites, the possible distortion modes and symmetry relationships amongst which have been analysed thoroughly in terms of group theory by Howard et al. [23]. Despite this theoretical grounding, however, high quality experimental crystallographic analysis is lacking in many of these systems. Bode et al. report $(NH_4)_3InF_6$ as crystallising in the tetragonal system, space group *P*4/*mnc* [24]. This is one of the straightforward distortional possibilities derived by Howard [23] based purely on octahedral tilting: the $a^0a^0c^+$ mode expressed in Glazer notation [25], resulting in a unit cell with Z=2 and $a\sim\sqrt{2}\,a_p$, $b\sim\sqrt{2}\,a_p$, $c\sim 2\,a_p$, where a_p represents the archetypal cubic pervoskite lattice (Fig. 2(a)). The present variant has a still larger (Z=4) and lower symmetry (monoclinic) unit cell, which is not considered by Howard, and is related to the above tetragonal cell by a further doubling of the unit cell volume, by the transformation matrix (10−1, 010, 101). We are unaware of any previous example of this particular type of distortion in a cryolite; a relatively common monoclinic variant does exist, for example in $(NH_4)_3ScF_6$, but this has a cell with Z=2, which is metrically close to the tetragonal variant. A comparison of β-$(NH_4)_3InF_6$ and α-$(NH_4)_3InF_6$, as reported by Bode [24], is given in Fig. 2. It can be seen that the octahedral tilt system is much more complex, with tilts allowed along all three pseudo-cubic axes; the principal contributions the additional lowering of symmetry arise from displacements of the fluorine atoms, a fact that was verified by a displacement mode analysis using the program ISODISPLACE [26]. It has been suggested [27] that the phase transitions in NH_4^+-based cryolites are order–disorder transitions driven by hydrogen-bonding requirements (as opposed to alkali metal based systems, which have phase transitions of the displacive type). In the present case, ordering of the NH_4^+ groups does indeed occur, with well-defined H-bonding contacts from each of the three crystallographically distinct NH_4^+ sites (Table 3, Fig. 3). The closest analogue to **2** which has been structurally characterised is $(NH_4)_2NaInF_6$ [28]. This is reported to adopt the 'parent' ordered

Table 3
Hydrogen bonding in β-$(NH_4)_3InF_6$ (**2**), distances (Å), angles (deg).

D–H	d(D–H)[a]	d(H···A)	< DHA	d(D···A)	A
N1–H1A	0.96	1.90	161	2.826	F4 [x, $-y+1/2$, $z+1/2$]
N1–H1B	0.91	1.82	169	2.717	F5 [$-x$, $y-1/2$, $-z+1/2$]
N1–H1C	0.90	1.85	168	2.736	F1 [$-x+1$, $-y$, $-z+1$]
N1–H1D	0.92	1.87	166	2.763	F6 [$-x$, $-y$, $-z$]
N2–H2A	0.89	1.93	178	2.813	F2 [x, $-y+1/2$, $z+1/2$]
N2–H2B	0.94	1.85	169	2.783	F2 [$-x+1$, $-y+1$, $-z+1$]
N2–H2C	0.84	1.95	163	2.761	F3 [$-x+1$, $-y$, $-z+1$]
N2–H2D	0.94	1.96	150	2.812	F4 [x, $-y+1/2$, $z+1/2$]
N3–H3A	0.80	1.91	172	2.710	F3 [$-x+1$, $-y$, $-z+1$]
N3–H3B	0.79	1.95	174	2.735	F6 [x, $-y+1/2$, $z+1/2$]
N3–H3C	0.92	1.88	173	2.794	F4
N3–H3D	0.96	2.19	130	2.898	F1 [$-x+1$, $-y+1$, $-z+1$]

[a] Standard uncertainties on D–H and A···H ca. 0.04 Å, on D···A ca. 0.005 Å, on < DHA ca. 4°.

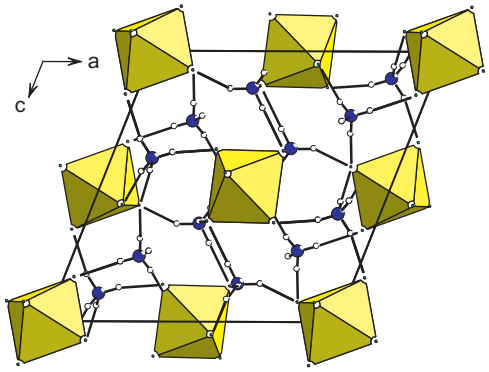

Fig. 3. Hydrogen bonding scheme in **2**; InF_6 drawn as polyhedra, all $(NH_4)^+$ cations drawn as ball-and-stick.

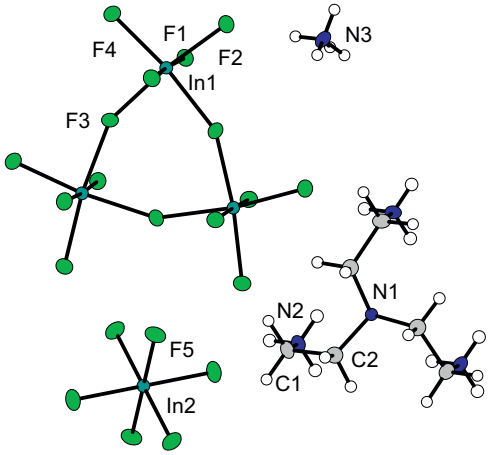

Fig. 4. Building unit in **3**, drawn with 50% probability ellipsoids.

double perovskite structure type (cubic, Fm-3m, $a \sim 2\ a_p$), albeit with ordering of the NH_4^+ groups. As indicated above, our PXRD data suggests that $(NH_4)_3InF_6$ adopts a higher symmetry polymorph at room temperature. We intend to carry out a thorough temperature-dependent structural phase diagram for $(NH_4)_3InF_6$ to ascertain the full sequence of phase transitions, which might be anticipated to be rich in detail.

3.3. $[NH_4]_3[C_6H_{21}N_4]_2[In_4F_{21}]$ (**3**)

Compound **3** is a new hybrid fluoride exhibiting novel structural features. The building unit contains two distinct In

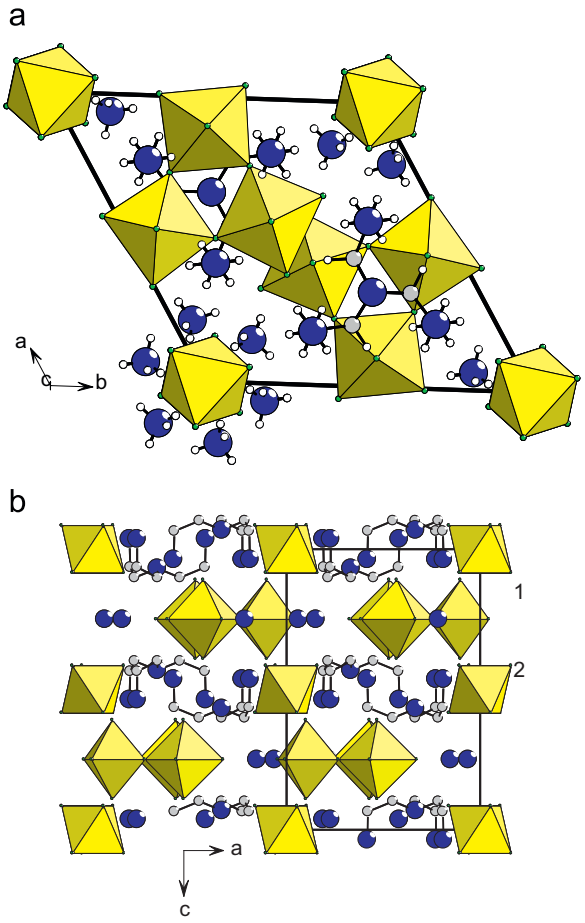

Fig. 5. (a) Crystal packing in **3**, viewed down the c-axis. H atoms not shown. (b) Crystal packing in **3**, viewed down the b-axis. Note the layer sequence along c: layers containing *tren* and InF_6 octahedra (1) alternate with layers containing NH_4^+ and $[In_3F_{15}]$ trimers (2).

sites, both of which have octahedral geometry (Table 2, Fig. 4). In(2) sits on a site of −3 symmetry with six equivalent In–F bonds, whereas In(1) sits on a mirror plane and forms a trimeric $[In_3F_{15}]^{6-}$ unit defined by the three-fold axis. The In(1)F_6 octahedron is slightly distorted, with an elongated bridging In–F bond and shorter terminal bonds. Crystal packing is shown in Fig. 5(a) and (b). It can be seen that there are no direct covalent interactions between the trimeric and monomeric In–F units, and that these are separated into alternating 'layers' along the c-axis. Moreover, there is segregation of the two different cationic species into these layers; *viz.* the NH_4^+ cations occur solely within the $[In_3F_{15}]^{6-}$ layer and the $[C_6H_{21}N_4]^{3+}$ cations solely within the $[InF_6]^{3-}$ layer. Inter-ionic H-bonds hold the structure together, with several strong N−H···F contacts in the region 2.65–2.72 Å. As shown in Fig. 6, there is a close matching between the 3-fold axes of the $[In_3F_{15}]^{6-}$ and $[C_6H_{21}N_4]^{2+}$ units and it is therefore tempting to conclude that the formation of the trimeric In–F unit is templated by the organic cation. Trimeric units are rather rare in metal fluoride chemistry; indeed this appears to be the first crystallised example of an isolated $[M_3F_{15}]$ unit, although related oxyfluoride trimers exist in $MoOF_4$, $TcOF_4$ [29] and $K[C_4H_{12}N][V_3O_3F_{12}]$ [30]. Although Na^+ was present in the reaction mixture it was not incorporated into the product. The *tren* shows partial breakdown to produce NH_4^+ *in situ*, however, it remains partially intact, unlike in the reaction for **2**, and also in the formation of $[NH_4]_2[Sc_3F_{11}]$ [8] under similar conditions. Both the latter reactions use water as solvent, so its absence may favour the stability and incorporation of *tren*.

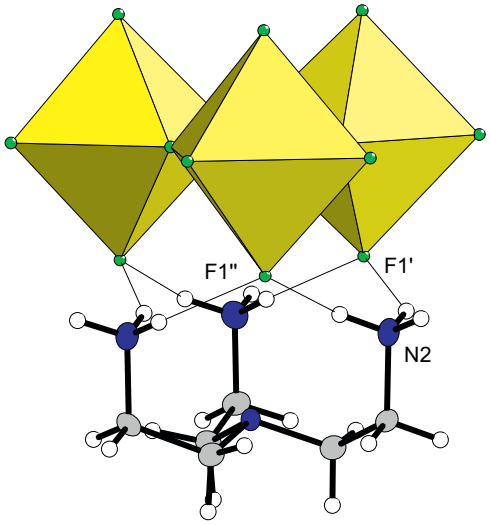

Fig. 6. H-bond mediated templating of the $[In_3F_{15}]$ unit by the *tren* moiety. H-bond distances N2···F1′=2.711(6) Å, N2···F1″=2.679(9) Å.

4. Conclusions

An exploration of the chemistry of indium in a variety of solvothermal systems has produced three compounds; the first two are previously known, but the crystal structures have not previously been reported. Compound **2**, in particular, has a new and noteworthy structural distortion within a well-known basic structural type, mediated by H-bonding requirements. Compound **3** is an unusual example of an inorganic–organic hybrid indium fluoride, with the *tren* moiety showing a genuine templating effect in directing the formation of a rare trimeric metal fluoride unit. Further exploratory studies of indium fluoride solvothermal chemistry are merited.

Supporting information available

Crystallographic information (cif files) and powder X-ray diffraction data.

Acknowledgments

We thank Prof. Alex Slawin for assistance with collection of the single crystal X-ray data and the University of St Andrews and EPSRC for funding.

Appendix A. Supplementary material

Supplementary data associated with this article can be found in the online version at doi:10.1016/j.jssc.2009.11.022.

References

[1] T. Loiseau, H. Muguerra, J. Marrot, G. Férey, M. Haouas, F. Taulelle, Inorg. Chem. 44 (2005) 2920.
[2] K. Adil, M. Leblanc, V. Maisonneuve, J. Fluorine Chem. 127 (2006) 1349.
[3] K. Adil, J. Marrot, M. Leblanc, V. Maisonneuve, Solid State Sci. 9 (2007) 531.
[4] F.H. Allen, Acta Crystallogr. B 58 (2002) 380.
[5] N.F. Stephens, P. Lightfoot, J. Solid State Chem. 180 (2007) 260.
[6] P. Lightfoot, N.F. Stephens, Mater. Res. Soc. Symp. Proc. 848 (2005) 13.
[7] N.F. Stephens, A.M.Z. Slawin, P. Lightfoot, Chem. Commun. (2004) 614.
[8] N.F. Stephens, P. Lightfoot, Solid State Sci. 8 (2006) 197.
[9] A.C.A. Jayasundera, A.A. Finch, P. Wormald, P. Lightfoot, Chem. Mater. 20 (2008) 6810.
[10] J. Touret, X. Bourdon, M. Leblanc, R. Retoux, J. Renaudin, V. Maisonneuve, J. Fluorine Chem. 110 (2001) 133.
[11] P. Bukovec, Monatsh. Chem. 114 (1983) 277.
[12] G.M. Sheldrick, Acta Crystallogr. A 64 (2008) 112.
[13] L.J. Farrugia, J. Appl. Cystallogr. 32 (1999) 837.
[14] C. Jacoboni, J.J. Leble, J. Rousseau, J. Solid State Chem. 36 (1981) 297.
[15] J. Grannec, J. Portier, P. Hagenmuller, J. Solid State Chem. 2 (1971) 227.
[16] W.T. Fu, D.J.W. Ijdo, J. Solid State Chem. 181 (2008) 1236.
[17] J. Ravez, M. Elaatmani, P. Hagenmuller, Mater. Res. Bull. 16 (1981) 1253.
[18] D.W. Aldous, P. Lightfoot, Solid State Sci. 11 (2009) 315.
[19] R.D. Shannon, Acta Crystallogr. A 32 (1976) 751.
[20] R.J. Goff, P. Lightfoot, submitted for publication.
[21] F.C. Hawthorne, R.B. Ferguson, Can. Miner. 13 (1975) 377.
[22] I.N. Flerov, M.V. Gorev, K.S. Aleksandrov, A. Tressaud, J. Grannec, M. Couzi, Mater. Sci. Eng. 24 (1998) 81.
[23] C.J. Howard, B.J. Kennedy, P.M. Woodward, Acta. Crystallogr. B 59 (2003) 463.
[24] B.H. Bode, E. Voss, Z. Anorg. Allg. Chem. 290 (1957) 1.
[25] A.M. Glazer, Acta Crystallogr. B 28 (1972) 3384.
[26] B.J. Campbell, H.T. Stokes, D.E. Tanner, D.M. Hatch, J. Appl. Crystallogr. 39 (2006) 607.
[27] I.N. Flerov, M.V. Gorev, J. Grannec, A. Tressaud, J. Fluorine Chem. 116 (2002) 9.
[28] A. Roloff, D. Trinschek, M. Jansen, Z. Anorg. Allg. Chem. 621 (1995) 737.
[29] A.J. Edwards, G.R. Jones, R.J.C. Sills, J. Chem. Soc. A (1970) 2521.
[30] M. Hilbers, M. Leimkuhler, R. Mattes, Z. Naturforsch. B 44 (1989) 383.